Structural Engineering and Mechanics, Vol. 39, No. 3 (2011) 361-382
DOI: http://dx.doi.org/10.12989/sem.2011.39.3.361

Efficacy of CFRP configurations for shear of RC beams: experimental and NLFE

Ahmed B. Shuraim*

College of Engineering (Civil), King Saud University, Riyadh, Saudi Arabia

(Received July 19, 2010, Accepted April 13, 2011)

Abstract. This paper presents the results of an investigation on shear strengthening of RC beams externally reinforced with CFRP composite. A total of six full-scale beams of four CFRP strengthened and two unstrengthened were tested in the absence of internal stirrups in the shear span. The strengthening configurations contained two styles: discrete uniformly spaced strips and customized wide strips over B-regions. The composite systems provided an increase in ultimate strength as compared to the unstrengthened beams. Among the three layouts that had the same area of CFRP, the highest contribution was provided by the customized layout that targeted the B-regions. A comparative study of the experimental results with published empirical equations was conducted in order to evaluate the assumed effective strains. The empirical equations were found to be unconservative. Nonlinear finite element (NLFE) models were developed for the beams. The models agreed with test results that targeting the B-region was more effective than distributing the same CFRP area in a discrete strip style over shear spans. Moreover, the numerical models predicted the contribution of different configurations better than the empirical equations.

Keywords: shear strengthening; reinforced concrete beams; CFRP; composite modeling; NLFE; empirical equations; externally bonded reinforcement

1. Introduction

There is a growing interest in the rehabilitating of existing reinforced concrete (RC) structures, where applications of FRP materials have been rapidly growing around the world. Common methods of shear strengthening of rectangular beams include wrapping the FRP system around three sides of the member (U-wrap) or bonding to the two sides of the member where the fibers in the FRP may also be orientated at different angles. Different strengthening schemes have been studied (see for example, Chaallal *et al.* 1998, Li *et al.* 2001, Khalifa and Nanni 2002, Chen and Teng 2003, Adhikary and Mutsuyoshi 2006, Barros *et al.* 2007, Mosallam and Banerjee 2007, Grande *et al.* 2007, Kim *et al.* 2008). In all wrapping schemes, the FRP system can be installed continuously along the shear span length of a member or placed as discrete strips.

While installing the strengthening systems over the shear span is the most common approach, an alternative approach is to target the B-region for strengthening for economical and efficient solution, especially for large members. According to ACI-318 (2008), the shear span of a beam is composed

*Corresponding author, Associate Professor, E-mail: ashuraim@ksu.edu.sa

of B-regions and D-regions. For such an unconventional approach, available predictive equations are not applicable; thus, an advanced method of analysis is needed for the structure before and after strengthening.

The nonlinear finite element (NLFE) method is the most general rational method that can be used for prediction of shear strength (ASCE-ACI 445), and it can be extended to model the behavior of the complete composite system. Technical literature on the composite modeling is replete with various elements and interface/bond assumptions (Perez *et al.* 2005, Godat *et al.* 2007, Lee *et al.* 2008, Kim and Vecchio 2008, Ibrahim *et al.* 2009, Gamino *et al.* 2009). Different approaches have been taken for the simulation of debonding failures in FRP-strengthened RC structures. Obviously, the success of any approach depends on the criteria adopted for defining the onset of debonding failures in FRP (Lu *et al.* 2006). It is extremely difficult to make any generalize solution for the shear strength enhancement of RC beams using external CFRP composite materials (Mosallam and Banerjee 2007).

This paper provides an investigation on shear strengthening of RC beams externally reinforced with CFRP composite using tests and NLFE. Two strengthening configurations were considered: discrete uniformly spaced strips and customized wide strips over B-regions. The tested beams were also analyzed using NLFE numerical models where simplified criteria for debonding were adopted. The experimental-numerical results were compared among each other and when applicable compared with available empirical equations. Good correlation among test and NLFE results were obtained.

2. Experimental program

2.1 Specimen design

The specimens were normal sized beams with a nominal thickness of 400 mm, a width of 200 mm, and a total length of 2.6 m with a shear span of 1200 mm. The overall shear span of the beam was three times the beam depth. Thus, based on ACI-318 definition of force discontinuity regions (D-Region), each shear span was composed of two D-regions and one B-region, each of which having a width of 400 mm. The beams were designed to be shear-deficient by not providing internal shear reinforcement; therefore, they are to be strengthened by U-shaped externally bonded CFRP. The details of the beams are shown in Fig. 1 through Fig. 3.

For beams BR600, SS200, and SS100, each shear span was covered by 600 mm CFRP sheet, comprising a continuous wide strip over each B-region, three 200-mm discrete uniformly spaced strips, and six 100-mm discrete uniformly spaced strips, respectively. For beams BR400 each shear span was covered by 400 mm CFRP sheet placed as a continuous strip over the B-region.

All of the beams contained the same bar size and spacing for the longitudinal reinforcement: 2 φ 22 mm (f_y = 568 MPa) at the bottom side and one 8 mm (f_y = 483 MPa) rebar at the top. Average concrete strength at 28 days from standard specimens, f_c', was 30 MPa. Technical properties of CFRP sheets were summarized in Table 2, as specified by the manufacturer data sheets.

The beams were cast in the same orientation as they were later tested. The specimens were wet cured for 7 days under layers of saturated burlap and plastic sheeting. The beams were then exposed to normal atmospheric conditions until the time of strengthening. The beams were strengthened after 30 days from the time of casting, and tested after 10 days from the time of installing the CFRP sheets.

2.2 Experimental setup

A typical beam was supported by full-width rollers placed at the ends while the load was applied over a plate located at the center of span. Each specimen was loaded with several load increments up to failure using displacement control and was measured by a loading cell. Instrumentation for each specimen was designed to capture the load-deformation response, strain in the reinforcing bars, and crack development. Instrumentation included vertical displacement measurements using LVDT under the loading point. Electrical strain gauges were placed on a number of rebars and on the CFRP surfaces, as shown in Fig. 2. Continuous recording of displacements and reinforcement strains and incremental loads were conducted throughout the loading history.

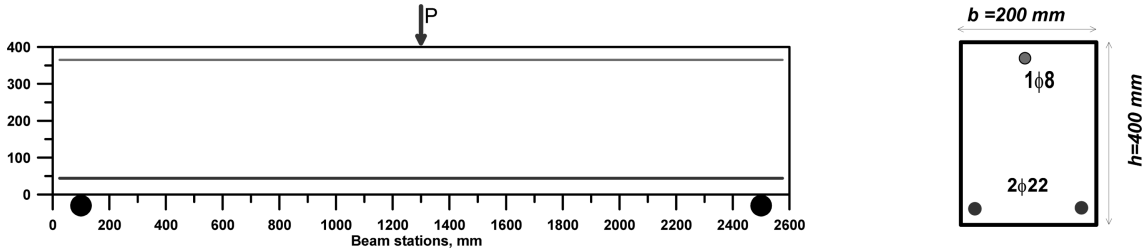

(a) Elevation (b) Cross section

Fig. 1 Details of unstrengthened beams (a) elevation, (b) cross section

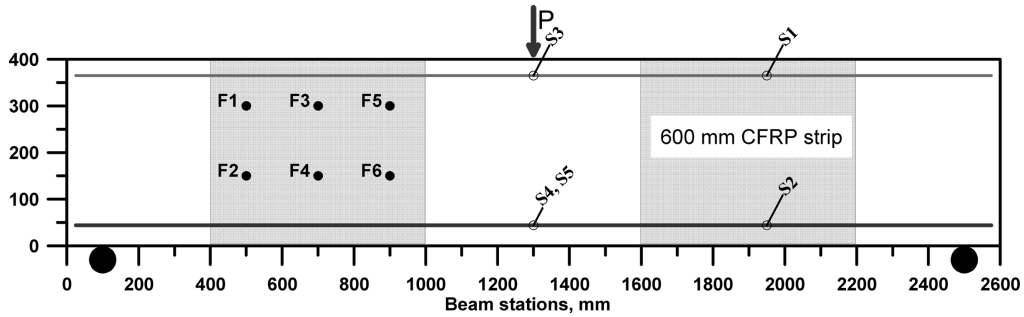

(a) BR600: one 600 mm strip on each side (total thickness =1200 mm)

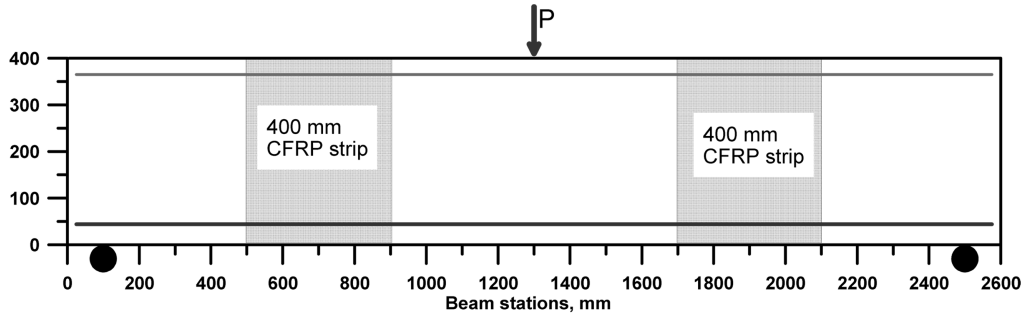

(b) BR400: one 400 mm strip on each side (total thickness =800 mm)

Fig. 2 Details of customized beams (a) BR600, (b) BR400

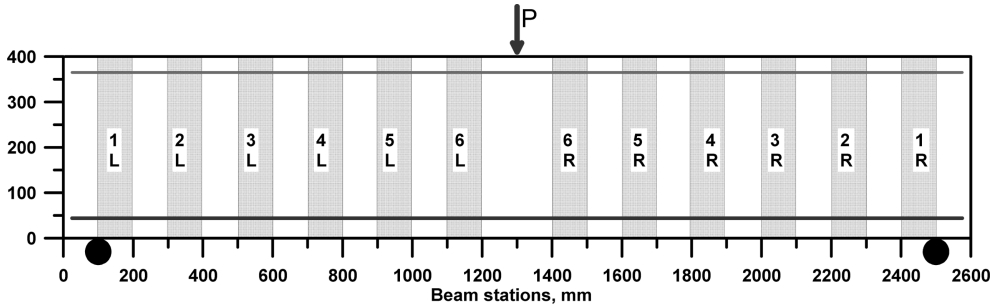

(a) SS100: six 100 mm strips on each side (total thickness =1200 mm)

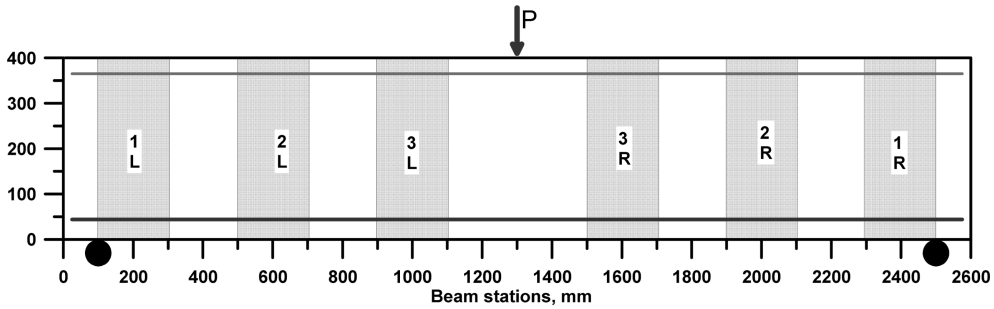

(b) SS200: three 200 mm strips on each side (total thickness =1200 mm)

Fig. 3 Details of discrete uniformly spaced strips beams (a) SS100, (b) SS200

Table 1 CFRP data from Manufacturer's data sheet

Property	Average value	Design value
Tensile strength, MPa	894	715
Tensile modulus, MPa	65402	61012
Tensile elongation, mm/mm	0.0133	0.0109
Ply Thickness, mm	0.381	

2.3 Material properties

Various externally bonded FRP reinforcement systems are available which differ depending on type of FRP, type of adhesive, method of curing, material preparations, etc. In this study, unidirectional carbon fiber reinforced polymer (CFRP) fabrics (SikaWrap Hex 230c) with the properties shown in Table 1 were utilized.

3. Finite element simulations of the behavior of concrete structures

3.1 Background

The physical behavior of concrete is very complex, being largely determined by the properties and interaction among its constituent materials. To incorporate these experimentally-observed features

into finite element, several constitutive modeling theories have been proposed, including: nonlinear elasticity, plasticity, and damage mechanics, among others (Chen and Han 1988, Grassl 2006, Nguyen 2008). The main components in the development of the classical theory of plasticity are: an initial yield surface, a hardening rule, and a flow rule. An initial yield surface in stress space defines the stress level at which plastic deformation begins. A hardening rule regulates the evolution of the subsequent loading surfaces during the course of plastic flow. A flow rule defines an incremental plastic stress- strain relationship using a plastic potential function (Chen and Han 1988).

To make plasticity formulation applicable to concrete, its components have been augmented by tension-cutoff surface, non-uniform hardening, non-associated flow, and pressure-dependent yield surface. Stiffness degradation and post-peak softening are among the challenging features for plasticity formulation, and for these features, the damage mechanics provides a consistent way for taking these features into consideration. Accordingly, a coupled damage-plasticity formulation can provide a better representation of salient concrete features (Grassl 2006, Nguyen 2008).

In this study, ABAQUS damage-plasticity model was chosen for modeling concrete behavior. This model assumes stiffness degradation due to damage is embedded in the plasticity part of the model using two independent scalar damage parameters. The post-peak in tension was represented by the fictitious crack model by Hillerborg (1985), which is characterized by three key parameters: the specific energy dissipated after the localization in the cracked region; the tensile strength in direct tension; and, the shape assumed for the softening branch. The energy criterion has been employed instead of strength failure criterion in order to minimize the superficial dependence on the chosen

Table 2 Equations for estimating concrete properties

Parameter	Equation	Reference
Fracture energy, G_f, where f_c' is the concrete compressive strength	$G_f = 110\left(\frac{f_c'}{10}\right)^{0.18}$	Fib Bulletin 42 (2008)
Direct tensile strength, f_t' (MPa)	$f_t' = 0.25\sqrt{f_c'}$	Naaman (2004)
Modulus of elasticity for concrete, E_c (MPa)	$E_c = 3000\sqrt{f_c'} + 6900$	ACI-363 (1997)
Post-cracking tensile curve for concrete, where n is a coefficient taken as 1.	$f_t = f_t'\left(1 - \frac{x}{d_0}\right)^n$ $d_0 = \frac{G_f(n+1)}{f_t'}$	Murthy (2009)
Concrete stress-strain relation in compressive	$\frac{f_c}{f_c'} = \frac{\beta\frac{\varepsilon}{\varepsilon_0}}{\beta - 1 + \left(\frac{\varepsilon}{\varepsilon_0}\right)^{\beta}}$ $\beta = \frac{1}{1 - \frac{f_c'}{\varepsilon_0 E_c}}$ $\varepsilon_0 = 0.001648 + 0.0000165 f_c'$	Carreira and Chu (1985)

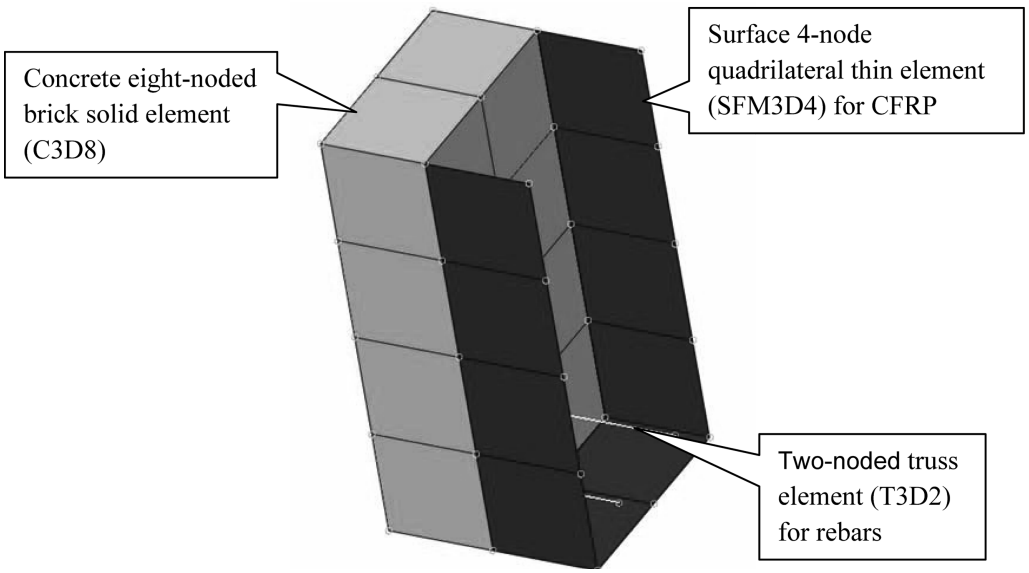

Fig. 4 Partial view of a beam showing the three main elements of the model (concrete element, CFRP element, and Rebar element)

finite element. Concrete can be modeled with a variety of 2-D and 3-D elements. In this study, eight-noded brick solid element (C3D8) was selected for concrete while a bi-linear elastic-plastic model was chosen for reinforcing steel and represented in space via two-noded truss elements (T3D2) as shown in Fig. 4.

3.2 Concrete parameters

The input parameters for the damage-plasticity model of concrete include the uniaxial compression curve, the uniaxial tensile strength, Poisson's ratio, modulus of elasticity, dilatancy angle, and the fracture energy. These parameters were defined as per available test data as well as from appropriate models from the technical literature. The equations in Table 2 were used as a general guideline for estimating material parameters in this study.

3.3 Composite modeling

For modeling the CFRP, a surface 4-node quadrilateral thin element named SFM3D4 was used which has no inherent stiffness, behave just like membrane elements with zero thickness and may be used with rebar layers. Through an internal numerical operation, the CFRP strip properties were attached to the SFM3D4 where the stiffness and mass of the CFRP sheets are added to the surface elements. In developing the model geometry, the SFM3D4 elements were meshed such that their nodal points coincide with the concrete nodal points where they attached, as shown in Fig. 4. By having common nodes with the concrete surface nodes, the assumption of perfect bond was imposed. The perfect bond assumption can be accurate for small strain; however, debonding will eventually occur when the strain reaches a critical value.

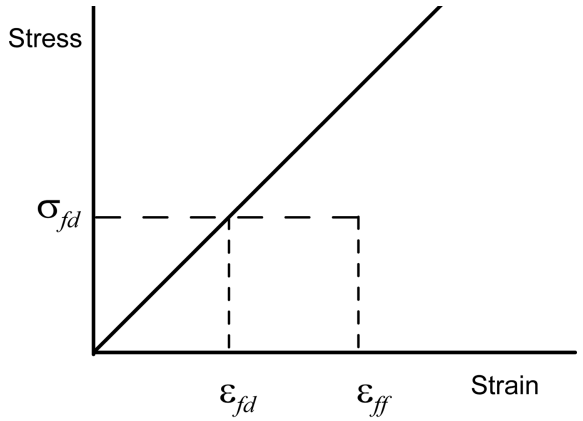

Fig. 5 CFRP stress-strain limits

The strengthening system was composed of CFRP strips acting as the strengthening material bonded to concrete via epoxy adhesive material which acts as the load transferring medium. Even though the carbon fibers have linear elastic properties, the composite action is controlled not only by the fibers but also by the transferring medium and the concrete strength and surface condition.

Therefore, as shown in Fig. 5, two limits were taken in this study to account for the onset of the debonding. When the strain at any integration point reaches the debonding strain, ε_{fd}, the stress reaches its maximum usable value, σ_{fd}. However, it was assumed that the stress can be maintained until reaching a failure strain, ε_{ff}. Previous studies (ACI-440, FIB-14, Triantafillou and Antonopoulos, and Matthys and Triantafillou) showed different values for the maximum usable strain in the FRP sheets for predicting the strengthening contribution without debonding. The value for ε_{fd} considered in this study was 0.004.

4. Results and discussions

4.1 Unstrengthened shear-deficient beams

4.1.1 Load-deflection curves

The results of two unstrengthened beams in terms of load-deflection relationships are shown in Fig. 6. This group of beams serves as control beams to establish a reference for the concrete shear strength of beams without internal stirrups or external CFRP strips. The failure loads were 132 kN, and 149.5 kN with an average value of 141 kN. The load-deflection from NLFE is shown along with the two experimental curves for the replicate beams. While the initial slope of the numerical curve is higher than the experimental curves, there is good agreement in predicting the maximum load and its deflection as well as the descending branch.

4.1.2 Concrete cracking and numerical tensile strains

The experimental result in terms of cracking failure for a typical unstrengthened beam is shown in Fig. 7. The beam is marked to identify the B and D regions where the width of each region is equal to the depth of the beam. It is well known that cracks form when the principal tensile stresses

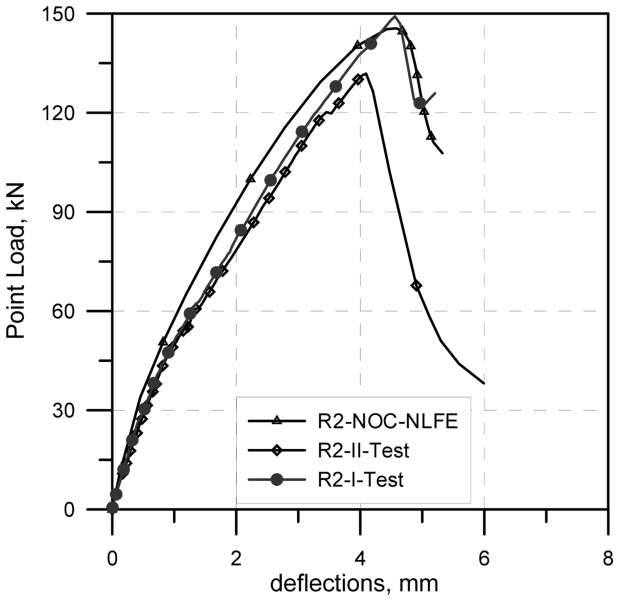

Fig. 6 Load-deflection curves for unstrengthened beams

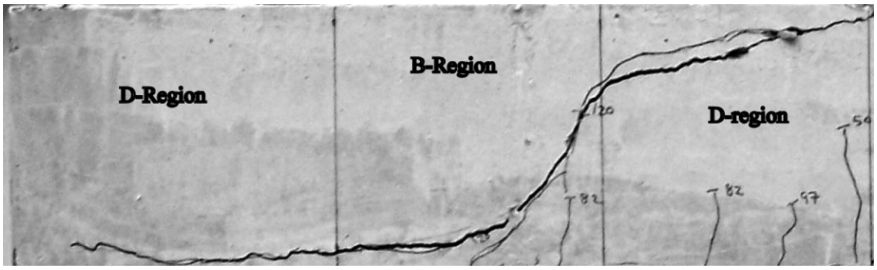

Fig. 7 Cracking pattern of unstrengthened beam

exceed the tensile strength of the concrete. In this beam, the first visible cracks were vertical flexural cracks just below the applied load, initiated from the bottom side. A major diagonal crack was developed in the B-region at approximately 45° to the axis of the member. At failure, splitting cracks parallel to the bottom flexural reinforcement became visible, and the diagonal crack extended to the loading point.

The NLFE numerical models formulated on the smeared crack approach do not produce actual physical cracks, however, strains or stresses can usually be interpreted to show the potential crack and load transfer mechanism. Fig. 8 shows the maximum plastic tensile concrete strain in a contour form and in symbolic form where the length of the arrowed- lines is an indication of the magnitude and the potential crack is to develop perpendicular to the line direction. A thorough examination of the magnitude and direction of these symbolic arrows indicates good qualitative agreement with the observed cracks in the tested beams and these observations can be used as a guide for placing the strengthening scheme.

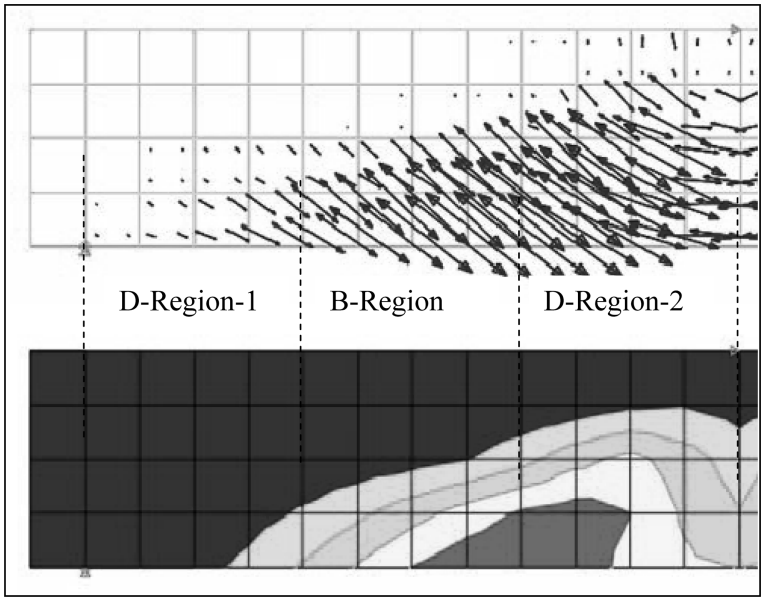

Fig. 8 Contours of maximum principal plastic strains in unstrengthened beam

4.1.3 Empirical equations

Technical literature contains a number of predictive equations for shear strength of RC beams without shear reinforcement that have been developed on the basis of statistical studies and regression analysis of a large number of data. In general, these equations contain several parameters that have been identified to affect shear strength; including: tensile strength of concrete as measured by the parameter $(f_c')^n$, where n may be taken as 1/2 or 1/3; longitudinal reinforcement ratio, ρ;

Table 3 Predictive equations for one-way shear strength of concrete

Reference	v_c	V_c, kN
ACI-318-08	$v_c = \frac{1}{6}\sqrt{f_c'}$	65
Eurocode-2-2004	$v_c = 0.18\left(1+\sqrt{\frac{200}{d}}\right)(100\rho f_{ck})^{1/3}$ where, $f_{ck} = f_c' - 1.60$ Mpa	70
Zsutty (1968)	$v_c = 2.2\left(f_c'\rho\frac{d}{a}\right)^{1/3}\left(\frac{2.56}{a}\right)$, where $\left(\frac{2.5d}{a}\right)\geq 1$	71.5
Kim and Park (1996)	$v_c = 3.5{f_c'}^{1/3}\rho^{2/8}\left(0.4+\frac{d}{a}\right)\left\{\frac{1}{\sqrt{1+0.008d}}+0.18\right\}$	67.8
Bentz (2005)	$V_c = \frac{200}{1000+s_a}\sqrt{f_c'}$; $S_e = 31.5\frac{dA}{a_g+16}$	68.84

Notes: a_g is the maximum aggregate size = 20 mm; ρ = 1.3%, f_c' = 30 MPa , d = 368 mm, a = 1200 mm.

and the shear span to depth ratio *a/d*. Size effect is considered in Eurocode 2 (2004) and also in the equation by Bentz (2005). A number of predictive equations were chosen as shown in Table 3 to compute the concrete shear strength for this group of beams without stirrups. The general form of a typical equation is

$$V_c = v_c b_w d \tag{1}$$

where v_c is the shear stress accounting for some of the influencing parameters, b_w is the beam width, d is the effective depth, and V_c is the shear force carried by concrete. Shear from the two tested control beams were V_{cT} = 66 kN and 74.75 kN with an average value of 70.5 kN, while the NLFE produced shear strength of V_{cN} = 72.8 kN. The average shear by predictive equations was 68.6 kN, thus, most of the equations provided good predictions.

4.2 Customized strips over B-regions (BR600 and BR400)

The basic data obtained from the tests were assembled and discussed in order to provide some insights into the composite action created by CFRP sheets and the reinforced concrete beams.

4.2.1 Load-deflection relationship

The load-deflection relationships for BR400 and BR600 are shown Fig. 9. The difference between the two beams is the width of the sheet coverage. While BR600 reached flexural capacity, BR400 failed in a brittle manner at a load that is 78 percent of the former beam. Prior to failure, however, the two beams were approximately identical.

For these layouts, the finite element numerical models were developed. The load-deflection curve for BR600 is plotted in Fig. 9 showing a maximum load capacity of the same magnitude as the experimental curve. According to the assumptions made in numerical model, the maximum stress in the CFRP sheets is that associated with a maximum strain of 0.004. Beyond this value, the strain

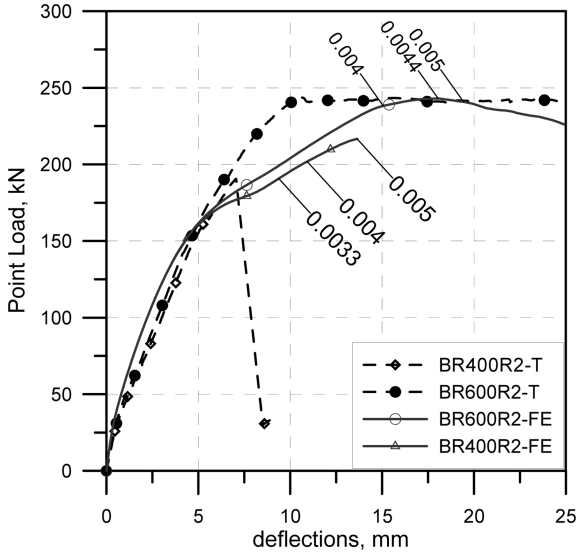

Fig. 9 Load-deflection relationship for BR400 and BR600

may increase without an increase in the stress. Three critical values of maximum strains in the CFRP sheets are also shown on the curve.

From the curve of BR600, the strain in CFRP reached a value of 0.004 when the load was 238.2 kN corresponding to 0.98 of the test load. The maximum load of 242.97 kN was reached when the maximum strain in the sheets was 0.0044, and the load of the beam decreased slightly at a strain of 0.005. For BR400, the value of 0.004 occurred when the load was 201.9 kN corresponding to 1.06 of the test load. The maximum load of 216.7 kN was reached when the maximum strain in the sheets was 0.005, while the closest prediction to test load was achieved when the maximum strain in the CFRP sheets was 0.0033. Comparing the experimental and the numerical curves for the beam BR400, it is reasonable to assume that the test beam failed before the strain reached 0.004. Based on the results of BR600 and, BR400 the limiting maximum strain in CFRP sheets of 0.004 provided good correlation with the test loads.

4.2.2 The state of strains over the shear strips

For any member subjected to shear loading, the strains over the height of concrete member is not uniformly distributed and thus, the bonded fibers are stressed differently and some fibers are relatively unstressed when the most stressed fiber reaches a critical level (Taljsten and Carolin 2007). This finding was confirmed by the strain distribution over the CFRP shear strips, experimentally and by NLFE numerical model as shown in Fig. 10 through Fig. 12. The contour of strains for BR 600 as obtained by NLFE numerical model is shown in Fig. 10, where the maximum strain is located in the lower side and the lowest strain is at the exterior upper corner. Experimentally, the strains were measured at six locations over one strip and the strain readings are shown in Fig. 11. The strains at the six locations varied in magnitude, where the largest measured strain was located at F6, and it exceeded 0.005. The strains at the other five locations did not exceed 0.003. The top row of strain gages exhibited much lower strains than the bottom counterparts. These strain readings in Fig. 11 are consistent qualitatively with the contours shown in Fig. 10.

For BR400, the distribution of strains over shear sheets is non-uniform as shown in Fig. 12. The maximum strain is in the lower side and the lowest strain is at the exterior upper corner. It should be recalled that the state of strains over the shear strips is a key parameter in the guidelines for shear strengthening design, whether it is for empirical equations or for NLFE modeling purpose.

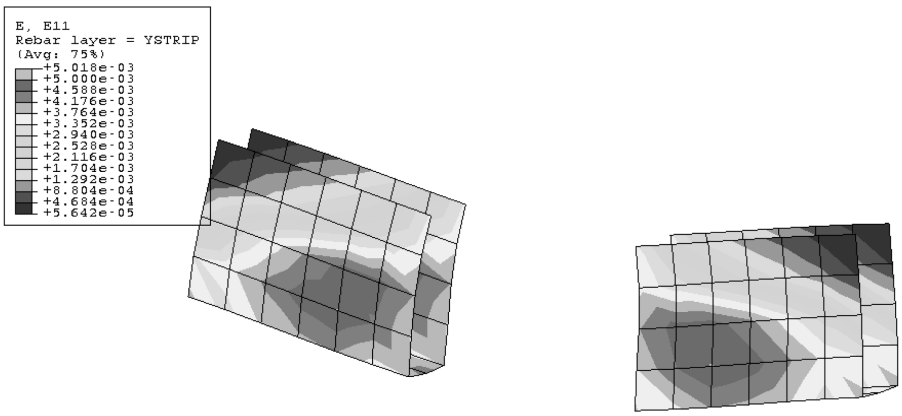

Fig. 10 Strain distribution in the CFRP strips for beam BR600

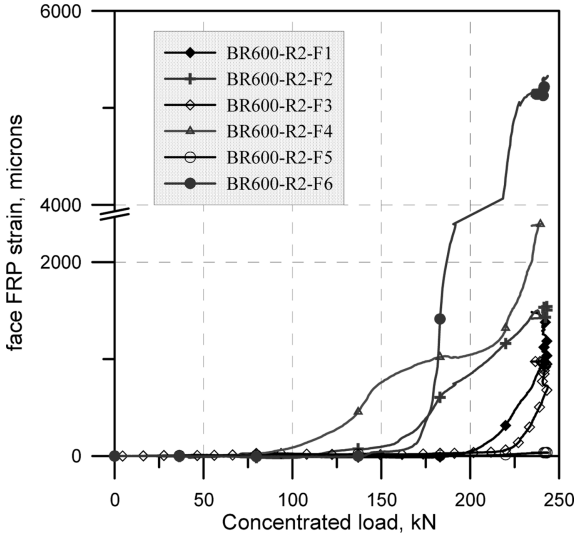

Fig. 11 Strain readings at identified locations for beam BR600

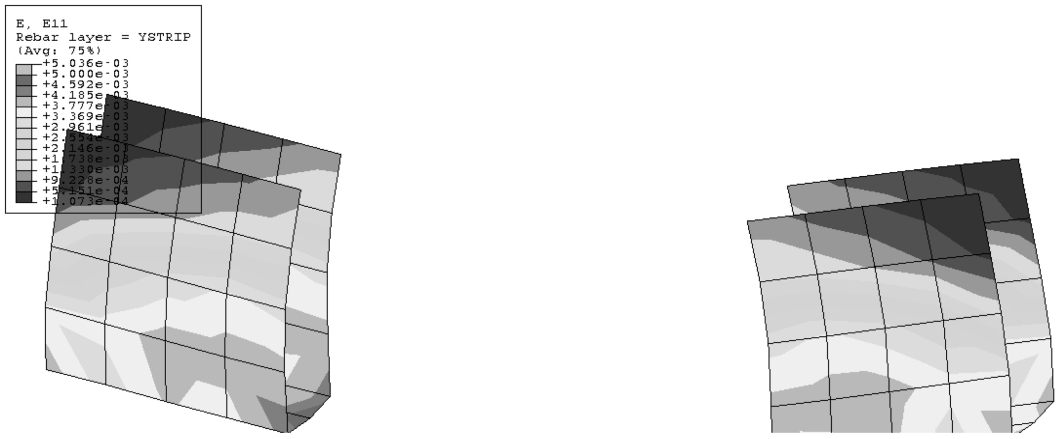

Fig. 12 Strain distribution in the CFRP strips for beam BR400

4.2.3 Concrete cracking and numerical tensile strains

As indicated earlier, the NLFE numerical models do not produce actual physical cracks; however, strains plotted in symbolic arrows can provide a qualitative assessment to the expected cracking patterns. The tensile principal plastic strains for BR600 are presented in symbolic arrowed-lines as shown in Fig. 13(a) where the length of the line is an indication of the strain magnitude and the orientation of the line is an indication of crack direction. However, it is well-recognized that the formation of cracks is more complex and that strains can be used as guidelines for potential cracking. Fig. 13(a) shows vertical arrows in the upper side of the middle region between the two wide CFRP strips; these arrows suggest a potential horizontal cracking, which was visible in the tested beam before full crushing of the top layer. Diagonal arrows in the exposed middle region are consistent with the visible shear-flexure inclined crack pattern in Fig. 13(b).

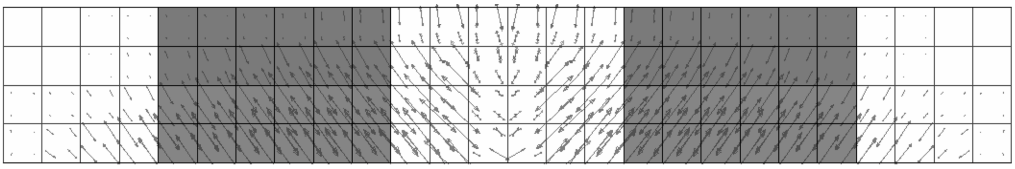

(a) Maximum tensile strains of concrete in symbolic form for beam BR600

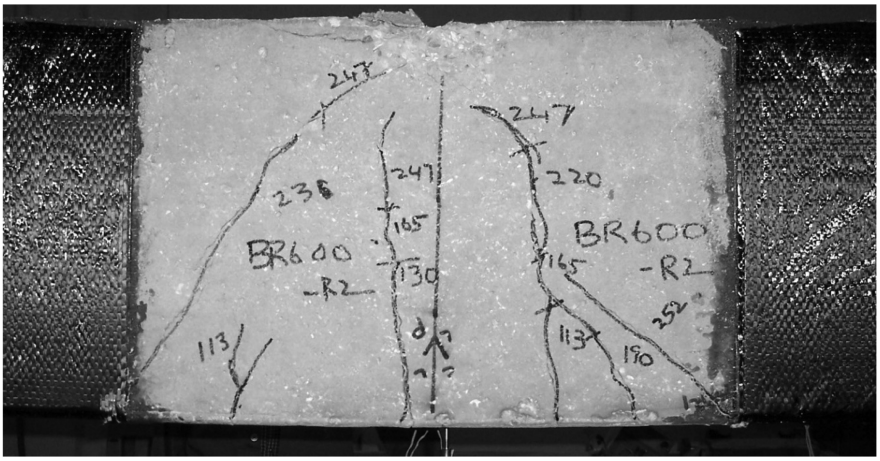

(b) Cracking pattern in beam BR600

(c) Cracking pattern in beam BR400

Fig. 13 Tensile plastic strain trajectory and observed cracking pattern for BR600 and BR400

For BR400, the general trend of the strain symbols is similar to that for BR600; however, the relatively narrower CFRP sheets were not able to prevent the initiation of diagonal crack. The crushing of the concrete at the upper side of the middle region between the two wide CFRP strips is consistent with the vertical symbols. The major diagonal flexural shear crack crosses the sheet over the upper portion causing debonding for the lack of sufficient anchorage length.

4.3 Discrete uniformly spaced strips (SS100 and SS200)

4.3.1 Load-deflection relationship

The load-deflection relationships for SS100 and SS200 are shown Fig. 14 and Fig. 15, respectively. The two beams have the same A_f/S_f ratio, but they differ in the fact that S_f/d_f ratio exceeds the limit of most design recommendations, where A_f is the strip area such that $A_f = 2t_f w_f$, where t_f is the sheet thickness, w_f is the strip width, and s_f is the longitudinal spacing. Both SS100 and SS200 failed in a brittle manner at a load that was 83 and 70 percent, respectively, of the BR600, which reached flexural capacity. The load-deflection relationships obtained from the NLFE numerical models are also shown Fig. 14 and Fig. 15 along with the experimental curves.

Similar to the previous models, three critical values of maximum strains in the CFRP sheets are shown on the NLFE curves. From the curve of SS200 in Fig. 14, the strain in CFRP reached a value of 0.004 when the load was 189 kN corresponding to 1.11 of the test load. The load reached a value of 204.27 kN when the maximum strain in the sheets was 0.005, while the closest prediction to test load achieved when the maximum strain in the CFRP sheets was 0.00215. For SS100 curve in Fig. 15, the strain in CFRP reached a value of 0.004 when the load was 200.5 kN corresponding to 1.04 of the test load. When the strain in the CFRP sheets was 0.005, the beam carried a load of 209.3 kN, while the closest prediction to test load achieved when the maximum strain in the CFRP sheets was 0.0041.

Based on the results of all tested beams, the limiting maximum strain in CFRP sheets of 0.004 provided good correlation with the test loads. The complexity of identifying a maximum strain limit for shear prediction is reflected in the various values proposed by previous studies (ACI-440 2008, FIB-14 2001, Triantafillou and Antonopoulos 2000, Matthys and Triantafillou 2001).

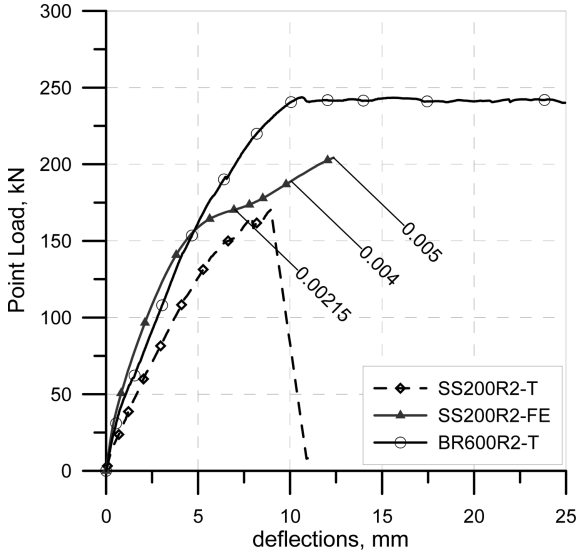

Fig. 14 Load-deflection relationship for BR600 vs. SS200 beams

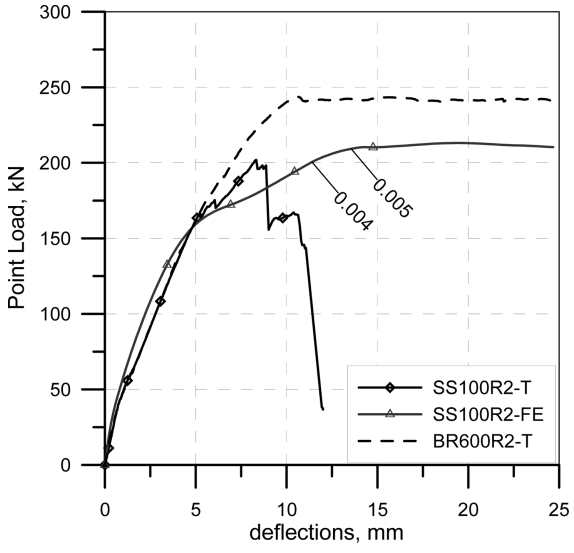

Fig. 15 Load-deflection relationship for BR600 vs. SS100 beams

4.3.2 The state of strains over the shear strips

As stated earlier, the strains over the height of concrete member subjected to shear loading are not uniformly distributed and thus, the bonded fibers are stressed differently (Taljsten and Carolin 2007). The findings from this study confirmed the above statement both experimentally and numerically. The contour of strains for SS200 as obtained by NLFE numerical model is shown in Fig. 16, which shows that the highest intensities of strains are located within the lower part of the interior strips (2R), which can qualitatively correlated with the rupture of the strips in Fig. 17. The upper part of the exterior strips is of marginal tensile strain which is consistent with the experimental observation where the upper portion is intact while the bottom portion is ruptured. Similar observations are noticeable for SS100 as shown in Fig. 18. Among the six strips per half span, the 4th and 5th strips are highly stressed at their lower parts, followed by the 3rd and the 2nd. The upper portions of the 1st to 4th have no tensile strains, while the 5th and 6th have moderate tensile strains.

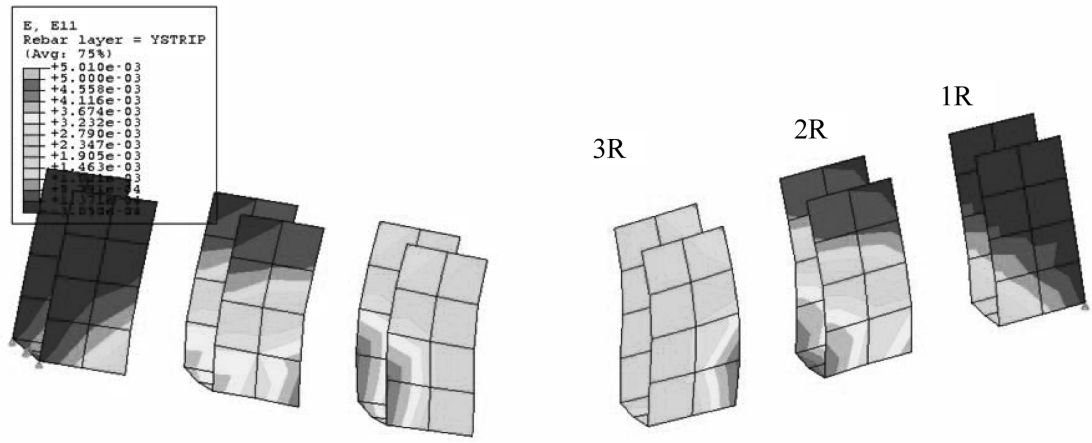

Fig. 16 Strain distribution in the CFRP strips for beam SS200

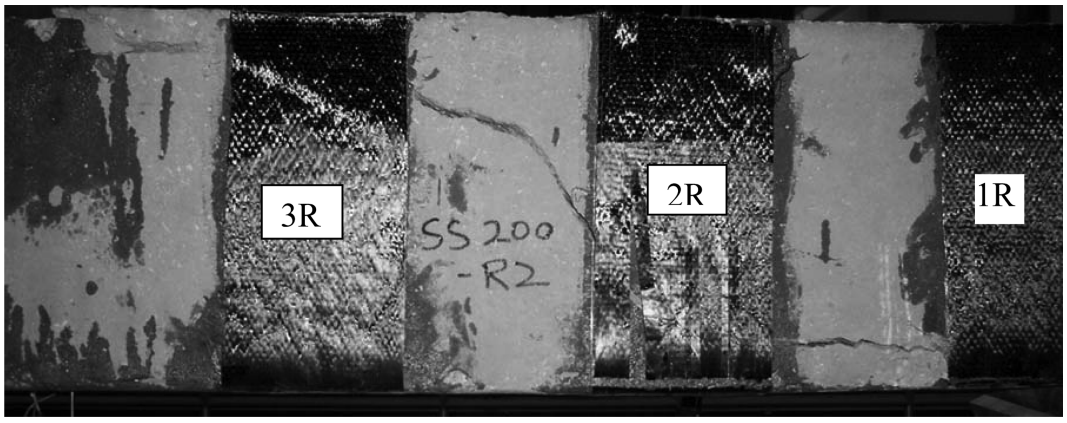

Fig. 17 Concrete tensile strain, cracking and failure of strips for SS200

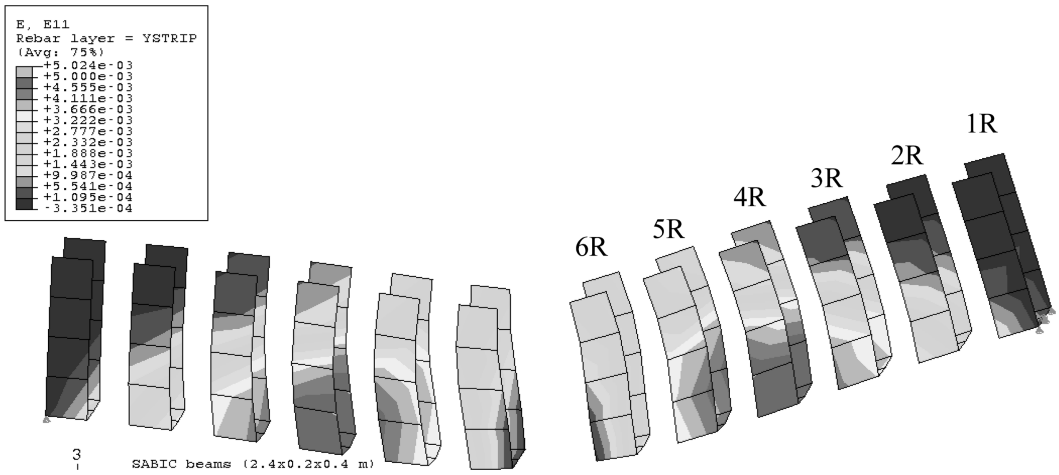

Fig. 18 Strain distribution in the CFRP strips for beam SS100

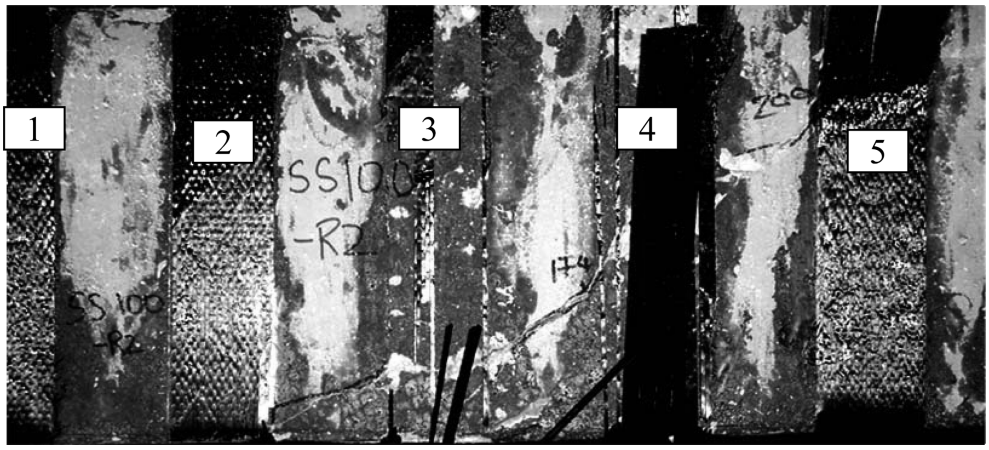

Fig. 19 Concrete tensile strain, cracking and failure of strips for SS100

4.3.3 Concrete cracking and numerical tensile strains

The tensile strains on the concrete surface can be correlated qualitatively with the cracking pattern as shown in Fig. 19 for SS200 and SS100. For SS200, the major crack crossed the first interior strip at the top where the anchorage length is limited and thus the strip provided limited resistance. The major crack crossed the middle strip in the lower part with ample anchorage length and thus the strip exposed to extensive damage and rupture at the bottom. It seems that the unrounded edge of the beam contributed to the damage.

For SS100, the major diagonal crack crosses three strips at different heights, causing peeling off and ruptures. Two of the damaged strips are in the B-region while one is at the boundary. The path of crack depends on parameters including the shear-span to depth ratio. For inadequate anchorage length for the strip crossed at the top, debonding occurred with little damage while for those with sufficient anchorage length rupture prevailed.

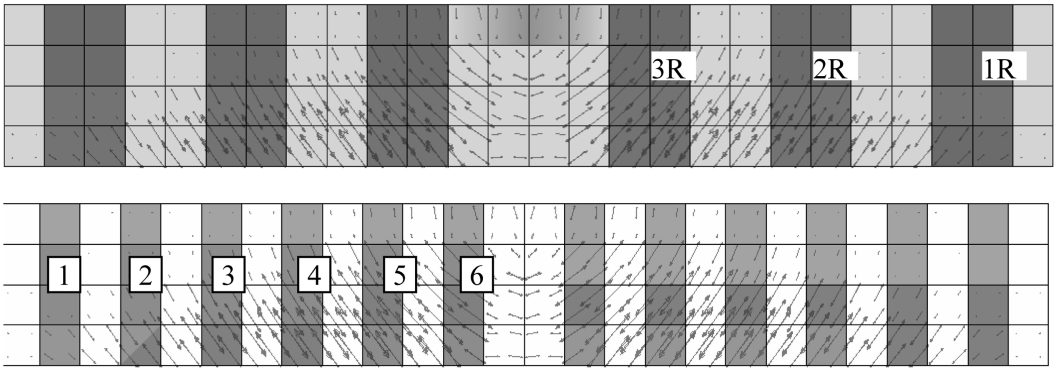

Fig. 20 Concrete tensile strain, for SS200 and SS100

5. Shear contributions of different layouts

5.1 Empirical equations

In most existing design proposals, the nominal shear strength, V_n, of an FRP-strengthened RC beam is evaluated from

$$V_n = V_c + V_s + V_f \tag{2}$$

Where, V_c, is the concrete contribution as discussed earlier.

The stirrup contribution to shear strength, V_s, has been formulated on the basis of modified truss model (ASCE-ACI 326 1962). For vertical stirrups, the contribution of stirrup is

$$V_s = \frac{A_v f_{yv} d}{S} \tag{3}$$

Where S is the longitudinal spacing of stirrups, A_v is the legs area, f_{yv} is the yield strength, and d is the effective depth of the section. In this study, no internal stirrups were included.

The contribution of FRP to shear capacity has been idealized in analogy with internal steel stirrups (ACI-440 2008, FIB-14 2001, Triantafillou and Antonopoulos 2000, Matthys and Triantafillou 2001, Taljsten and Carolin 2007). For vertical fibers, the contribution of FRP strips may be expressed as

$$V_f = k_f \frac{A_f f_{fe} d_f}{S_f} \tag{4}$$

Where the factor, k_f = 0.85 in ACI-440 for U-wrap and k_f = 0.72 in FIB-14. f_{fe} is the effective design stress in the strip such that $f_{fe} = \varepsilon_{fe} E_f$, and d_f is the effective depth of the strip. E_f is the modulus of elasticity, and ε_{fe} is defined using various expressions shown in Table 4.

In the ACI-440 equations, the effective strain is calculated using a bond-reduction coefficient k_v applicable to shear which relies on two modification factors, k_1 and k_2, that account for the concrete strength and the type of wrapping scheme used, respectively. it is also dependent on an active bond length, L_e, which is the length over which the majority of the bond stress is maintained.

Table 4 Empirical design equations

Method and results	Relevant equations	Additional equations
ACI-440 ε_{fe} = 0.004; V_f= 33.6 kN	$\varepsilon_{fe} = k_v \varepsilon_{fu} \le 0.004$ $k_v = \frac{k_1 k_2 L_e}{11900\,\varepsilon_{fu}} \le 0.75$	$L_e = \frac{23300}{(n_f t_f E_f)^{0.58}}$ $k_1 = \left(\frac{f_c'}{27}\right)^{2/3}$ $k_2 = \frac{d_f - L_s}{d_f}$
FIB-14 and Triantafillou and Antonopoulos (T&A) model ε_{fe} = 0.0074 V_f = 47.26 kN (FIB-14) V_f= 55.80 kN (T & A)	Choose the minimum value of $\varepsilon_{fe} = 0.17\left(\frac{(f_c')^{2/3}}{E_f \rho_f}\right)^{0.30} \varepsilon_{fu}$ $\varepsilon_{fe} = 0.00065\left(\frac{(f_c')^{2/3}}{E_f \rho_f}\right)^{0.56}$	$\rho_f = 2\frac{t_f w_f}{b_w S_f}$
Matthys and Triantafillou (Ms & T) model ε_{fe} = 0.00627 V_f= 52.6 kN (M & T)	$\varepsilon_{fe} = 0.56\,\varepsilon_{fu} e^{-0.0455\Gamma_f}$	$\Gamma_f = \frac{E_f \rho_f}{\left(\frac{a}{d}\right)(f_c')^{2/3}}$

5.2 Experimental and NLFE contributions

Experimentally, the shear forces carried by the stirrups, V_f were extracted using Eq. (5).

$$V_f \ge V_{uT} - V_{cT} \tag{5}$$

where V_{cT} is the concrete shear failure of the reference case taken as the average of two unstrengthened beams, while V_{uT} is the shear failure of the strengthened beams. Numerically, the shear forces carried by the stirrups, V_f were extracted using Eq. (6).

$$V_f \ge V_{uN} - V_{cN} \tag{6}$$

where, V_{cN} is the concrete shear failure of the control unstrengthened beam, while V_{uN} is the shear failure of the strengthened beams. The results from NLFE are summarized in Table 5, where the load was computed based on a limiting strain of 0.004 in the CFRP sheets.

Table 5 Contribution of CFRP by NLFE

Beam	Failure load, P, kN	V_{uN}, kN	V_{cN}, kN	V_f, kN	Strength ratio with respect to BR600
SS100	200.5	100.25	72.8	27.5	0.59
SS200	188.98	94.5	72.8	21.7	0.47
BR400	201.93	101	72.8	28.2	0.6
BR600	238.2	119.1	72.8	46.3	1

Table 6 Comparison of CFRP contributions

Test results				V_f					
Beam	Failure load, P, kN	V_{uT}, kN	V_{cT}, kN	Test, kN **(ratio of BR600)**	NLFE, kN	ACI-440, kN	FIB14, kN	T&A, kN	M&T, kN
SS100	201.9	100.95	70.5	30.45 **(0.60)**	27.5	33.6	47.26	55.80	52.6
SS200	170.4	85.20	70.5	14.7 **(0.29)**	21.7	33.6	47.26	55.80	52.6
BR400	190.6	95.30	70.5	24.8 **(0.49)**	28.2	N/A	N/A	N/A	N/A
BR600	243.1	121.55	70.5	51.05 **(1)**	46.3	N/A	N/A	N/A	N/A

5.3 Comparisons and discussions

The results in terms of CFRP contribution from test, NLFE and empirical predictive equations are summarized in Table 6. Test and NLFE showd that the system adopted for beam BR600 was the most effective, where 600 mm of CFRP was placed over each of the B-regions in the beam. The discrete-strips system applied to beams (SS100, SS200) had the same total width as BR600; however, they showed much less contributions than BR600 and among the two beams SS200 was the lowest. BR400 had two-third of the CFRP materials used in the previous three beams where 400 mm of CFRP was placed over each of the B-regions in the beam. Its contributions are 0.49 and 0.6 of BR600 as obtained from test and NLFE, respectively.

The high efficiency of BR600 may be attributed to placing the CFRP where they needed most as illustrated by the initiation of major diagonal crack in Fig. 7 and the strain contours in Fig. 8. In both figures, the most vulnerable area is the interior part of the B-region and part of the D-region-2. Thus covering these vulnerable parts is essential for high efficacy, which was accomplished in BR600 to a great degree. Other layouts produced less coverage to these critical areas.

It is to be noted that test results and NLFE agreed in trend and to a great extent in magnitude in terms of the load carrying capacity and the CFRP contribution of the four configurations.

On the empirical equations, they are applicable to discrete strips and strictly speaking when the spacing limitation is met, which may apply only to SS100. Nevertheless, the key element in the empirical equations is the assumed effective strain, where the equations in produce high values. ACI-440 shows the best prediction among the four analytical methods considered in this study.

6. Conclusions

The results of an investigation on shear strengthening of RC beams externally reinforced with CFRP composite were presented where a total of six full-scale beams were tested and numerically simulated using NLFE. Conventional discrete uniformly spaced strips over the shear spans and nonconventional strips that targeted B-regions were employed. Three-dimensional nonlinear finite element numerical models were developed using plasticity-damage approach in ABAQUS for

concrete modeling, elastic-plastic for rebars, and elastic with debonding criteria for CFRP. Appropriate meshing and material assumptions were employed. A comparative study of the experimental results with published empirical equations was conducted. Based on the findings of this study, the following remarks can be made.

1. The composite systems provided an increase in ultimate strength as compared to the unstrengthened beams. Among the three layouts that had the same area of CFRP, the NLFE models and the test results showed that targeting the B-regions was more effective than distributing the same CFRP area in a discrete strip style over shear spans. The least effective configuration was that involving discrete uniformly spaced strips with a large spacing to depth ratio.
2. NLFE models developed in this study with the stated assumptions showed good capabilities in identifying critical aspects of the behavior of tested beams. In unstrengthened beams, the model identified the weak areas and the potential cracking paths and the load-carrying capacity. In the strengthened beams, the models identified the load-carrying capacity and the strains distributions in the CFRP strips.
3. The contributions of the discrete strips were much less than what were predicted by the available empirical equations, in part because the assumed effective strains provided by the empirical equations were higher than should be. ACI-440 showed the best prediction among the four design methods considered in this study. Additional studies are needed to address the stress and strain limitations of CFRP for predicting the CFRP contribution when using empirical equations or when using NLFE.

Acknowledgements

The author gratefully acknowledges the support provided by SABIC under Grant No.428-36. Any opinions, findings, and conclusions expressed in this paper are those of the writer and do not necessarily reflect the views of the sponsor.

References

ACI Committee 318 (2008), "Building code requirements for structural concrete (ACI 318-08) and commentary", American Concrete Institute, Farmington Hills, MI.

ACI Committee 363 (1997), "State of the art report on high strength concrete (ACI 363R-92)", American Concrete Institute, Farmington Hills, MI.

ACI Committee 440.2R (2008), "Guide for the design and construction of externally bonded FRP systems for strengthening concrete structures", American Concrete Institute, Farmington Hills, MI.

Adhikary, B.B. and Mutsuyoshi, H. (2006), "Shear strengthening of reinforced concrete beams using various techniques", *Constr. Build. Mater.*, **20**, 366-373.

Ahmed, S.H. (1981), "Properties of confined concrete subjected to static and dynamic loading", Ph. D. Thesis, University of Illinois at Chicago.

ASCE-ACI Committee 326 (1962), "Shear and diagonal tension", *ACI J. Proc.,* **59**(1), 1-30, **59**(2), 277-334, **59**(3), 352-396.

ASCE-ACI Committee 426 (1987), The Shear Strength of Reinforced Concrete Members, ACI Committee Report ASCE-ACI 426R-74 (Reapproved 1980), Part 4 of ACI Manual of Concrete Practice, American Concrete Institute, Farmington Hills, MI.

ASCE-ACI Committee 445 (1998), "Recent approaches to shear design of structural concrete", *J. Struct. Eng.*, **124**(12), 1375-1417.
Barbato, M. (2009), "Efficient finite element modeling of reinforced concrete beams retrofitted with fiber reinforced polymers", *Comput. Struct.*, **87**, 167-176.
Barros, J.A.O., Dias, S.J.E. and Lima, J.L.T. (2007), "Efficacy of CFRP-based techniques for the flexural and shear strengthening of concrete beams", *Cement Concrete Compos.*, **29**, 203-217.
Bentz, E.C. (2005), "Empirical modeling of reinforced concrete shear strength size effect for members without stirrups", *ACI Struct. J.*, **102**(2), 232-241.
Carreira, D.J. and Chu, K.H. (1985), "Stress-strain relationship for plain concrete in compression", *ACI J. Proc.*, **82**, 797-804.
Chaallal, O., Nollet, M. and Perraton, D. (1998), "Shear strengthening of RC beams by externally bonded side CFRP strips", *J. Compos. Constr.*, **2**, 111-113.
Chen, J.F. and Teng, J.G. (2003), "Shear capacity of FRP-strengthened RC beams: FRP debonding", *Constr. Build. Mater.*, **17**, 27-41.
Chen, W.F. and Han, D.J. (1988), *Plasticity for Structural Engineers*, Springer-Verlag, New York.
Eurocode 2 (2004), Design of Concrete Structures, Part 1-1: General Rules and Rules for Buildings, 2004-1-1.
Fib Bulletin 14 (2001), "FRP as externally bonded reinforcement of R.C. structures: basis of design and safety concept", Technical Report by Task Group 9.3, The International Federation for Structural Concrete (fib), Lausanne, Switzerland.
Fib Bulletin 42 (2008), "Constitutive modeling of high strength/high performance concrete", State-of-art report by Task Group 8.2, International Federation for Structural Concrete (fib), Lausanne, Switzerland.
Gamino, A.L., Bittencourt, T.N., e Sousa, JLADO (2009), "Finite element computational modeling of externally bonded CFRP composites flexural behavior in RC beams", *Comput. Concrete*, **6**(3), 187-202.
Godat, A., Neale, K.W. and Labossiere, P. (2007), "Numerical modeling of FRP shear-strengthened reinforced concrete beams", *J. Compos. Constr.*, **11**(6), 640-649.
Grande, E., Imbimbo, M. and Rasulo, A. (2007), "Experimental behavior of RC beams strengthened in shear by FRP sheets", FRPRCS-8 University of Patras, Patras, Greece, July.
Grassl, P. and Jirasek, M. (2006), "Damage-plastic model for concrete failure", *Int. J. Solids Struct.*, **43**, 7166-7196.
Hillerborg, A. (1985), "The theoretical basis of a method to determine the fracture energy GF of concrete", *Mater. Struct.*, **8**, 291-296.
HKS (2005), ABAQUS - Users Manuals and Theory Manual Version 6.6, Pawtucket, RI, USA.
Ibrahim, A.M. and Mahmood, M.S. (2009), "Finite element modeling of reinforced concrete beams strengthened with FRP laminates", *Eur. J. Sci. Res.*, **30**(4), 526-541.
Khalifa, A. and Nanni, A. (2002), "Rehabilitation of rectangular simply supported RC beams with shear deficiencies using CFRP composites", *Constr. Build. Mater.*, **16**, 135-146.
Kim, G., Sim, J. and Oh, H. (2008), "Shear strength of strengthened RC beams with FRPs in shear", *Constr. Build. Mater.*, **22**, 1261-1270.
Kim, J.K. and Park, Y.D. (1996), "Prediction of shear strength of reinforced concrete beams without web reinforcement", *ACI Mater. J.*, **93**(3), 213-222.
Kim, S.W. and Vecchio, F.J. (2008), "Modeling of shear-critical reinforced concrete structures repaired with fiber-reinforced polymer composites", *J. Struct. Eng.*, **134**(8), 1288-1299.
Lee, H.K., Ha, S.K. and Afzal, M. (2008), "Finite element analysis of shear-deficient RC beams strengthened with CFRP strips/sheets", *Struct. Eng. Mech.*, **30**(2), 247-261.
Li, A., Diagana, C. and Delmas, Y. (2001), "CRFP contribution to shear capacity of strengthened RC beams", *Eng. Struct.*, **23**, 1212-1220.
Lu, X.Z., Jiang, J.J., Teng, J.G. and Ye, L.P. (2006), "Finite element simulation of debonding in FRP-to-concrete bonded joints", *Constr. Build. Mater.*, **20**, 412-424.
Matthys, S. and Triantafillou, T. (2001), "Shear and Torsion strengthening with externally bonded FRP reinforcement", *Proceedings of the International Workshop on: Composites in Construction: A Reality*, ASCE, Reston, VA.
Mosallam, A.S. and Banerjee, S. (2007), "Shear enhancement of reinforced concrete beams strengthened with

FRP composite laminates", *Compos. Part B*, **38**, 781-793.
Murthy, R.C., Palani, G.S. and Riyer, R. (2009), "State-of-the-art review on fracture analysis of concrete structural components", *Sadhana*, **34**(2), 345-367.
Naaman, A.E. (2004), *Prestressed Concrete Analysis and Design: Fundamentals*, Techno Press, 2nd edition, 1072.
Nguyen, G.D. and Korsunsky, A.M. (2008), "Development of an approach to constitutive modeling of concrete: Isotropic damage coupled with plasticity", *Int. J. Solids Struct.*, **45**, 5483-5501.
Taljsten, B. and Carolin, A. (2007), "Beams strengthened in shear by EBR – design model", FRPRCS-8 University of Patras, Patras, Greece, July.
Triantafillou, T.C. and Antonopoulos, CP. (2000), "Design of concrete flexural members strengthened in shear with FRP", *J. Compos Construct, ASCE* **4**(4), 198-205.
Zsutty, T.C. (1968), "Beam shear strength prediction by analysis of existing data", *ACI J.*, **65**(11), 943-951.